Numerical Optimization of an Annular Field Reversed Configuration Translation Experiment

IEPC-2009-008

Presented at the 31st International Electric Propulsion Conference
University of Michigan Ann Arbor, Michigan USA
September 20-24, 2009

Carrie S. Niemela* and Lyon B. King†
Michigan Technological University, Houghton, MI 49931

Abstract: Annular field reversed configuration (AFRC) devices form annular plasma toroids between a pair of concentric cylindrical coils. This plasmoid remains detached from the external magnetic field so that it can be ejected from the coils, making AFRCs viable pulsed inductive plasma accelerators. Though numerous formation studies on AFRCs are available, no successful translation studies have been published. Michigan Technological University, in conjunction with the Air Force Research Laboratory, is investigating the translation of AFRCs as pulsed inductive plasma accelerators. The first step in this investigation is to develop an annular electromagnetic launcher model to study the basic translation characteristics of the device. The launcher model treats the plasmoid as a rigid conducting slug, accelerated out of the coils by a Lorentz force. It predicts coil and plasmoid currents, plasmoid trajectories, and acceleration efficiencies for various input conditions. The model has been optimized for peak acceleration efficiency using a combination of non-dimensional analysis, genetic algorithms, and gradient-based numerical optimization routines. A description of the model, explanation of the numerical optimization techniques, and preliminary results from the model are presented in this paper.

Nomenclature

η^*_{accel} = Acceleration efficiency [non-dimensional]
η_{accel} = Acceleration efficiency
C_1 = Circuit capacitance
I^*_1 = Outer coil current [non-dimensional]
I^*_2 = Inner coil current [non-dimensional]
I^*_3 = Plasmoid current [non-dimensional]
I_0 = Coil circuit current
I_1 = Outer coil circuit current
I_2 = Inner coil circuit current
I_3 = Plasma circuit current
k_{13} = Outer coil-plasmoid coupling coefficient
k_{23} = Inner coil-plasmoid coupling coefficient
L_1 = Outer coil inductance
L_2 = Inner coil inductance
L_3 = Plasmoid inductance
L_e = External circuit inductance

*Ph.D. Candidate, Michigan Technological University, csniemel@mtu.edu
†Associate Professor, Michigan Technological University, lbking@mtu.edu

L_{e1} = Outer coil circuit external inductance
L_{e2} = Inner coil circuit external inductance
m = Plasmoid mass
M_{13} = Mutual inductance (Outer coil-plasmoid)
M_{23} = Mutual inductance (Inner coil-plasmoid)
n_i = Plasma density
n_{13} = Exponential power (Outer coil-plasmoid)
n_{23} = Exponential power (Inner coil-plasmoid)
R_1 = Outer coil circuit external resistance
R_2 = Inner coil circuit external resistance
R_3 = Plasmoid resistance
R_e = External circuit resistance
t = Time
t^* = Time [non-dimensional]
T_e = Electron temperature [eV]
u_z^* = Plasmoid velocity [non-dimensional]
u_f^* = Final plasmoid velocity [non-dimensional]
u_f = Final plasmoid velocity
u_z = Plasmoid velocity
V_c^* = Capacitor voltage [non-dimensional]
V_0 = Capacitor charging voltage
V_c = Capacitor voltage
z = Plasmoid position
z^* = Plasmoid position [non-dimensional]
z_{13} = Coupling scale length (Outer coil-plasmoid)
z_{23} = Coupling scale length (Inner coil-plasmoid)
z_{s13} = Profile z shift (Outer coil-plasmoid)
z_{s23} = Profile z shift (Inner coil-plasmoid)

I. Introduction

Annular field reversed configuration (AFRC) devices offer significant potential as high power electric propulsion technology. They form robust, high-energy density compact plasma toroids at relatively low energies (∼250 J). These plasmoids have a completely self-contained magnetic field structure which allows them to be expelled from their formation chamber at high velocity, similar to the pulsed inductive thruster[1](PIT) and conical theta pinch thruster.[2] Michigan Technological University (MTU), in conjunction with the Air Force Research Laboratory (AFRL), is constructing an experiment to study the behavior of translating AFRCs. This experiment, the TeXOCOT, is a next-generation device of AFRL/University of Michigan's XOCOT experiment[3] and AFRL's XOCOT-T experiment.[4]

The TeXOCOT program intends to measure the translation properties of an AFRC plasmoid, including its velocity, momentum, and acceleration efficiency. A new AFRC translation experiment for taking these measurements will be constructed in MTU's Ion Space Propulsion Lab. This experiment is being designed with the aid of an annular electromagnetic launcher model to identify a set of operating conditions, such as cone angle, circuit charging voltage, plasmoid mass, etc., for which translation of the plasmoid is possible and acceleration efficiency of the plasmoid is maximized. This paper presents the annular electromagnetic launcher model and optimization techniques used on the model to find the peak acceleration efficiency of an AFRC plasmoid. Preliminary findings from these methods indicate promising results, though further refinement is necessary.

II. Background: Annular Field Reversed Configurations

An annular field reversed configuration is a compact plasma toroid formed in the annular region between two coaxial coils, as shown in Figure 1. The purely poloidal B-field is supported by an induced toroidal (azimuthal) current. This diamagnetic current forms a closed magnetic field to confine the plasma. AFRCs were first proposed by Phillips[5] as a low-voltage formation method for fusion plasma, but subsequent research

at the University of Washington on the Coaxial Slow Source (CSS)[6] showed temperatures and densities in an AFRC are insufficient for fusion.

Formation of AFRCs remains an empirical process which is not well-understood, despite numerous studies.[3,7,8] The plasma is turbulent fluid, subject to complex magnetohydrodynamic instabilities requiring numerical plasma studies to resolve. Despite the limitation, the formation of AFRCs can be illustrated by considering basic electromagnetic principles.

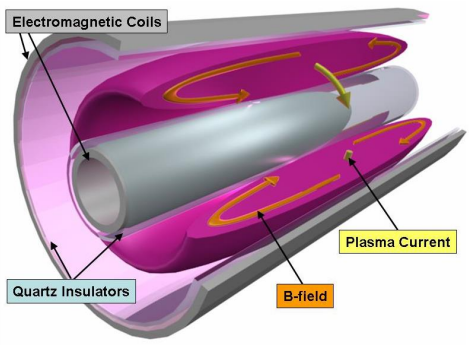

Figure 1. AFRCs are formed inductively between two coaxial coils as shown.

Annular FRCs can either be formed with the coils connected in parallel or the coils operating independently from one another. The parallel formation method will be the subject of this work; a dissertation by Smith[9] contains a detailed description of the independent coil mode. Figure 2 displays the circuit configuration, typical current waveforms, and the formation sequence for the parallel coil operation. The channel between the coils is filled with an inert gas (Step 1), which is then partially ionized or pre-ionized (Step 2). Upon completion of the pre-ionization stage, the capacitors are discharged into the coils adding oppositely directed magnetic fields in the annulus between the coils (Step 3). As a consequence of Faraday's Law, the rising currents in the coils cause a current to develop in the plasma, opposing this change in field (Step 4). This current is diamagnetic so that it creates a closed **B**-field topology to confine the plasma. Further increasing the currents in the coils causes the current in the plasma to increase, ionizing and heating it. External magnetic pressure from both coils balances with the plasma pressure to help keep the toroid well-centered in the annulus. Confinement of the plasma is improved if oppositely directed field lines near the coil ends are allowed to tear and reconnect, though evidence of this remains unclear.

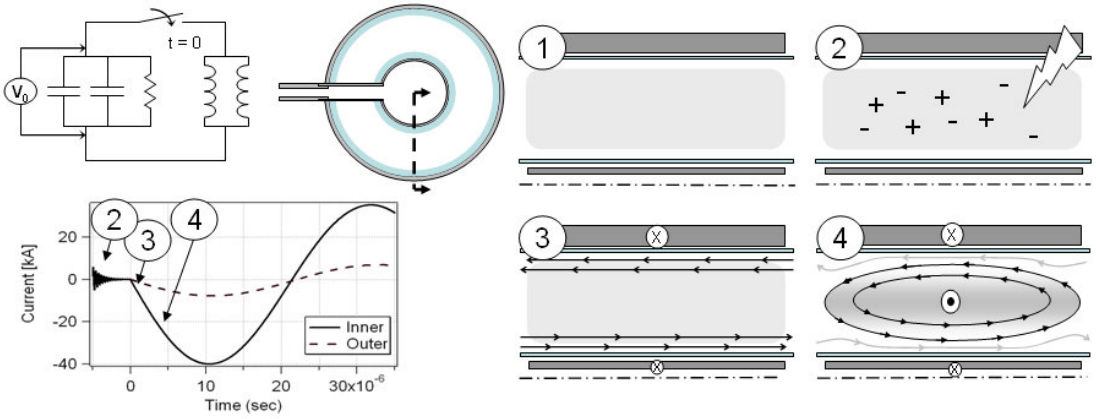

Figure 2. Parallel coil configuration showing circuit diagrams, schematics, and typical current waveforms. The formation sequence starts with a neutral backfill (1) followed by a pre-ionization of the fill gas (2). Current is pulsed through the coils (3) and the plasma current develops to oppose the change in B-field, resulting in a closed confinement (4).

Successful translation studies on AFRCs are not readily available. The XOCOT-T experiment attempted to translate the plasmoid, however evidence of translation was not apparent. In principle, AFRCs can be translated the same way as their close relative, the FRC.[10] Traditional FRCs do not use a center coil and operate on much faster ($\sim$5 μs) timescales. Most FRC devices translate the plasmoid using a conical outer coil in place of the traditional cylindrical coil. This creates a small radial magnetic field component which crosses with the azimuthal plasma current to create an axially directed Lorentz force. This method has been used successfully in the FRX/C-T,[11] the MTF experiment,[12] and was the translation method for the XOCOT-T.[4]

The Lorentz force acting on the plasmoid must be sufficiently large to overcome the plasmoid inertia and

it must accelerate the plasmoid in time comparable to the lifetime of the configuration. For AFRCs, the configuration typically lasts only about 20-30 μs.[6] Once translation of the plasmoid is initiated, the plasmoid can only be expelled from the formation chamber if it is completely detached from the magnetic field of the coil. Since the magnetic field null is along the centerline of the annulus in the parallel coil configuration, the plasmoid should always remain detached from the coils.

III. Annular Electromagnetic Launcher Model

Dynamic circuit models are a popular method for predicting the translation physics of a pulsed inductive plasmoid accelerators[1,13,14,15] and electromagnetic launchers.[16] These models couple the circuit equations with Newton's law, producing a set of simultaneous equations to describe the coupled electrical and dynamic behavior of the system. In short, they simplify the device down to a collection of circuit elements which can be solved using first order ordinary differential equations rather than computationally intense particle codes.

Similar to other models, the annular electromagnetic launcher model treats the plasmoid as a rigid conducting slug accelerated by a Lorentz force. This simplification masks the AFRC formation where the plasmoid is changing in shape as external magnetic field pressure balances with internal plasma pressure. Instead, it assumes that equilibrium is reached and the plasmoid maintains a constant shape. The model also neglects the expansion that occurs when the plasmoid leaves the coils, since this expansion for an AFRC has not been investigated.

The AFRC plasmoid forms inductively and is magnetically coupled to the coils through mutual inductance, which decays as it leaves the coils. The mutual inductance controls the Lorentz force by determining the interaction of the plasma current and the coil current. The currents can be calculated using circuit diagrams. Figure 3 provides a pictorial overview of the annular electromagnetic launcher model, operating in the parallel coil mode.

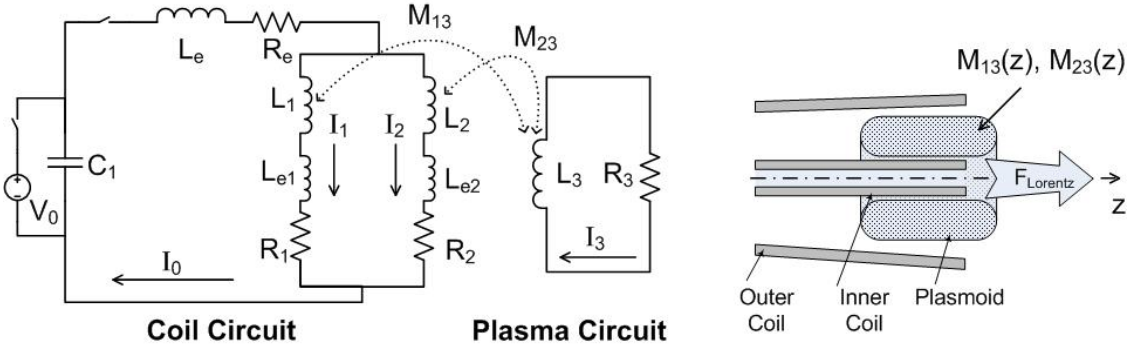

Figure 3. Schematic of the annular electromagnetic launcher model. The plasmoid is depicted with circuit elements L_3 and R_3, magnetically coupled to the coils through M_{13} and M_{23}.

The equations of motion for the plasmoid can be derived by calculating the Lorentz force from **J**x**B**, but this requires solving several intense integrals. A much easier and equivalent description can be found from conservation of energy, considering how the energy of the system changes as the plasmoid travels out of the coils. Magnetic field energy will change as the mutual inductance changes. This change in magnetic field energy can be related to Newton's 2nd Law through the work-kinetic energy theorem ($F_z = -\delta U/\delta z$), giving:

$$m\frac{du_z}{dt} = -\frac{dM_{13}}{dz}I_1 I_3 - \frac{dM_{23}}{dz}I_2 I_3 \tag{1}$$

where

$$u_z = \frac{dz}{dt} \tag{2}$$

In this model, position of the plasmoid z is tracked with regard to the trailing edge and $z = 0$ occurs at the small cone end of the coils. Computing I_1, I_2, and I_3 requires a circuit analysis of the system, yielding the following equations:

$$V_C(t) = L_e\frac{dI_0}{dt} + R_eI_0 + (L_1 + L_{e1})\frac{dI_1}{dt} + R_1I_1 - I_3\frac{dM_{13}}{dz}u_z - M_{13}\frac{dI_3}{dt} \tag{3}$$

$$I_0 = I_1 + I_2 \tag{4}$$

$$0 = (L_1 + L_{e1})\frac{dI_1}{dt} + R_1I_1 + (M_{23} - M_{13})\frac{dI_3}{dt} + \left(\frac{dM_{23}}{dz} - \frac{dM_{13}}{dz}\right)u_zI_3 - (L_2 + L_{e2})\frac{dI_2}{dt} - R_2I_2 \tag{5}$$

$$0 = R_3I_3 + L_3\frac{dI_3}{dt} - M_{13}\frac{dI_1}{dt} - I_1\frac{dM_{13}}{dz}u_z - I_2\frac{dM_{23}}{dz}u_z - M_{23}\frac{dI_2}{dt} \tag{6}$$

$$\frac{dV_C}{dt} = -\frac{I_0}{C_1} \tag{7}$$

The time derivatives of M_{13} and M_{23} in Equations 3, 5, and 6 have been separated into a positional derivative and velocity using the chain rule. Their profiles $M_{13}(z)$ and $M_{23}(z)$ as well as the coil and plasmoid inductances L_1, L_2, and L_3 are determined from the coil and plasmoid geometry. Given the coil radii, lengths, cone angle, and plasmoid geometry, the mutual inductance profiles $M_{13}(z)$ and $M_{23}(z)$ and L_1, L_2, L_3 can be calculated using analytical equations, experimental methods, or electromagnetic field solvers. As multiple authors have discovered[1,14,17] , the $M(z)$ profile satisfies an exponential distribution, similar to:

$$M(z) = k_0\sqrt{L_pL_c}\exp\left(-\left(\frac{|z - z_{shift}|}{z_{scale}}\right)^n\right) \tag{8}$$

where k_0 is the coupling coefficient, L_p and L_c are the plasmoid and coil inductances (L_3 and L_1 or L_2), z_{scale} is the coupling scale length, n is the exponential power term, and z_{shift} is the location of maximum $M(z)$. The difference in geometry between the outer coil-plasmoid combination and the inner coil-plasmoid combination will results in different coupling for both systems, meaning that for each geometry combination, the coefficients k_0, z_{scale}, z_{shift}, n will have unique values (k_{13}, k_{23}, z_{13}, z_{23}, z_{s13}, z_{s23}, n_{13}, n_{23}). It has been found that for large cone angles (greater than 10 °), n approaches 1 and z_{shift} is zero. For small cone angles, n and z_{shift} increase with decreasing cone angle.

Plasmoid resistance R_3 and plasmoid mass m can be estimated by assuming a fully ionized plasma with uniform properties of density n_i and temperature T_e. Resistivity then arises as a result of Coloumb collisions of the current carrying electrons with stationary ions. Spitzer[18] reports this resistivity for a diamagnetic plasma (like that in an AFRC) in terms of the ion charge number Z, the electron temperature (in eV) T_e, and the Coloumb logarithm $\ln\Lambda$:

$$\rho_{Spitzer} = 1.03 \times 10^{-4}\frac{Z\ln\Lambda}{T_e^{3/2}} \tag{9}$$

For an AFRC, $\ln\Lambda$ of 12-15 can be used. Using the estimated resistivity, plasma resistance can be calculated from $R = \rho l/A$, where l is the plasmoid length and A is the cross sectional area. The plasmoid mass, using the assumption of a uniform density, is then estimated as: $m = n_iVM_m/N_A$, where V is the plasmoid volume, M_m is the molar mass of the plasmoid gas, N_A is Avogadro's number.

Acceleration efficiency of the plasmoid can be defined as the final plasmoid kinetic energy compared to the energy initially stored in the capacitor bank:

$$\eta_{accel} = \frac{mu_f^2}{C_1V_0^2} \tag{10}$$

In this work, acceleration efficiency is the figure of merit; optimization of the model will focus on finding its maximum.

The launcher model is an initial value problem, requiring the values for I_1, I_2, I_3, V_c, u_z, and z to be specified at $t = 0$. These 6 initial conditions, combined with the 7 independent circuit elements (C_1, L_e, R_e, L_{e1}, L_{e2}, R_1, R_2), 4 coil geometry parameters (outer coil radius, outer coil cone angle, inner coil radius, coil length), 2 plasma geometry parameters (height, width), and 2 plasma properties (n_i, T_e), require that 21 inputs be specified for the model. This large parameter set takes 5 minutes to solve on a single-core processor, with the bulk of the time consumed calculating $M_{13}(z)$ and $M_{23}(z)$.

IV. Methodology

The long computation time and large number of inputs make optimization of the annular electromagnetic launcher model challenging. Reduction of the computational overhead can be achieved by removing the geometry dependence from the model and optimizing L_1, L_2, L_3, $M_{13}(z)$, and $M_{23}(z)$ independently. When these optimal parameters are found, a coil and plasmoid geometry can be fit to them. This method, however, does not ensure that the optimal L_1, L_2, L_3, $M_{13}(z)$, and $M_{23}(z)$ can produce a valid geometrical solution. To increase the likelihood of a valid output, the model equations can be non-dimensionalized so that scaling relations between parameters are developed. Optimization of the scaling relations results in generalized solutions to which may satisfy several geometries. Also, if the constraints on the output of the optimization routine are relaxed so that it locates several acceptable extrema rather than producing a single output, the chance of finding a valid geometrical solution is further increased.

These ideas were implemented in this work. First, the model equations in Section III were non-dimensionalized to put the solutions in terms of generalized scaling relations. This also brought the solution time for a single set of parameters down to a few seconds. Next, the non-dimensional equations were optimized for peak acceleration efficiency using a genetic algorithm. The genetic algorithm found sets of scaling relations with high efficiencies, greater than a predefined limit. These sets were then sorted according to efficiency and the best ones were further optimized with the gradient method. The optimized scaling relations dictate the relationships that circuit elements in the model should have to obtain peak efficiencies. Circuit elements were found from these solutions by substituting typical values into the relations, producing a set of dimensional parameters (i.e. L_e, C_1, L_1,etc). Since several of these dimensional parameters are dependent on the coil and plasmoid geometry, a geometry needed to be fit to these values. This fitting process is largely trial-and-error, where different combinations of coil-plasmoid geometries are inserted into the dimensional form of the model (presented in Section III) and the governing equations (Eq. 1 - 7) are numerically integrated to find the resulting acceleration efficiency. It is not always possible to satisfy each parameter exactly, but if the acceleration efficiency predicted by the launcher model is close to (or better than) the efficiency found using the optimization techniques, it is considered a good solution. Details of the non-dimensionalization process, optimization routines, and evaluation of the dimensional model are detailed in the following sections.

A. Non-Dimensional Model

The annular electromagnetic launcher model can be non-dimensionalized by expressing the independent variables and dependent variables as non-dimensional terms: $t^* = t/t_0$, $z^* = z/z_0$, $u_z^* = u_z/u_0$, $V^* = V/V_0$, $I_1^* = I_1/V_0\sqrt{L_e/C_1}$, $I_2^* = I_2/V_0\sqrt{L_e/C_1}$, and $I_3^* = I_3/V_0\sqrt{L_e/C_1}$. Here $u_0 = z_0/t_0$. The variables t_0 and z_0 are time and length scales, which will be defined later. Substituting these into Equations 1 - 7 and forming groups reduces the system to the following non-dimensional equations:

$$\frac{du_z^*}{dt^*} = -\alpha\left(\frac{dk_{13}}{dz^*}\sqrt{\theta_1\theta_3}I_1^*I_3^* + \frac{dk_{23}}{dz^*}\sqrt{\theta_2\theta_3}I_2^*I_3^*\right) \tag{11}$$

$$\frac{dz^*}{dt^*} = u_z^* \tag{12}$$

$$V_c^* = \frac{1}{\tau_0}\left[\left(\tau_0\gamma_e\right)\left(I_1^* + I_2^*\right) + \left(1 + \theta_1 + \theta_{e1}\right)\frac{dI_1^*}{dt^*} + \frac{dI_2^*}{dt^*} + \gamma_1\tau_0 I_1^* - k_{13}\sqrt{\theta_1\theta_3}\frac{dI_3^*}{dt^*} - \frac{dk_{13}}{dz^*}\sqrt{\theta_1\theta_3}I_3^*u_z^*\right] \tag{13}$$

$$0 = (\theta_1 + \theta_{e1}) \frac{dI_1^*}{dt^*} - (\theta_2 + \theta_{e2}) \frac{dI_2^*}{dt^*} + \gamma_1 \tau_0 I_1^* - \gamma_2 \tau_0 I_2^* + \left(k_{23} \sqrt{\theta_2 \theta_3} - k_{13} \sqrt{\theta_1 \theta_3} \right) \frac{dI_3^*}{dt^*} + \left(\frac{dk_{23}}{dz^*} \sqrt{\theta_2 \theta_3} - \frac{dk_{13}}{dz^*} \sqrt{\theta_1 \theta_3} \right) I_3^* u_z^* \tag{14}$$

$$0 = \theta_3 \frac{dI_3^*}{dt^*} + \gamma_p \tau_0 I_3^* - k_{13} \sqrt{\theta_1 \theta_3} \frac{dI_1^*}{dt^*} - k_{23} \sqrt{\theta_2 \theta_3} \frac{dI_2^*}{dt^*} - \left(\frac{dk_{13}}{dz^*} \sqrt{\theta_1 \theta_3} I_1^* + \frac{dk_{23}}{dz^*} \sqrt{\theta_2 \theta_3} I_2^* \right) u_z^* \tag{15}$$

$$\frac{dV_c^*}{dt^*} = -\tau_0 \left(I_1^* + I_2^* \right) \tag{16}$$

The new non-dimensional groups are defined as:

$$\gamma_e = R_e \sqrt{\frac{C_1}{L_e}} \quad \gamma_1 = R_1 \sqrt{\frac{C_1}{L_e}} \quad \gamma_2 = R_2 \sqrt{\frac{C_1}{L_e}} \quad \gamma_p = R_3 \sqrt{\frac{C_1}{L_e}} \tag{17}$$

$$\alpha = \frac{V_0^2 C_1}{m \left(z_0 / t_0 \right)^2} \quad \tau_0 = \frac{t_0}{\sqrt{L_e C_1}} \tag{18}$$

$$\theta_1 = \frac{L_1}{L_e} \quad \theta_2 = \frac{L_2}{L_e} \quad \theta_3 = \frac{L_3}{L_e} \quad \theta_{e1} = \frac{L_{e1}}{L_e} \quad \theta_{e2} = \frac{L_{e2}}{L_e} \tag{19}$$

Applying non-dimensional parameters $\sigma_{13} = z_0/z_{13}$, $\sigma_{23} = z_0/z_{23}$, $\sigma_{s13} = z_{s13}/z_0$, and $\sigma_{s23} = z_{s23}/z_0$, the coupling coefficients become:

$$k_{13}(z^*) = k_{13}^0 \exp\left(-\left(\left| z^* - \sigma_{s13} \right| \sigma_{13} \right)^{n_{13}} \right) \tag{20}$$

$$k_{23}(z^*) = k_{23}^0 \exp\left(-\left(\left| z^* - \sigma_{s23} \right| \sigma_{23} \right)^{n_{23}} \right) \tag{21}$$

where k_{13}^0 and k_{23}^0 are the nominal coupling coefficients for the outer coil-plasmoid and inner coil-plasmoid, respectively. The non-dimensionalization reduces the 22 original variables to 19 non-dimensional variables. Writing acceleration efficiency (Equation 10) in non-dimensional terms yields:

$$\eta_{accel}^* = \frac{\left(u_f^* \right)^2}{\alpha} \tag{22}$$

For this model, if the plasmoid cannot leave the coils during its lifetime it is considered to have a final velocity of zero and no acceleration efficiency. Setting z_0 to the coil length and t_0 as the confinement time, only parameters which satisfy the relation $z^*(t^* = 1) \geq 1$ will be considered as solutions.

B. Model Optimization: Genetic Algorithms and Gradient Based Methods

Genetic algorithms are a common technique for optimizing large parameter sets which contain many singularities, several local extrema, and non-differentiability. Since the annular electromagnetic launcher model has many parameter sets where the plasmoid fails to translate (singularities) and can have several maxima, a genetic algorithm is appropriate for this problem. Genetic algorithms use processes similar to genetic evolution to optimize a cost function (also called an objective function or fitness function). The algorithm starts by randomly selecting sets parameters. Each parameter is referred to as a chromosome. Each set of chromosomes form an individual and a group of individuals make up a generation. Each individual is then evaluated using a fitness function. In this case, the chromosomes for each individual are used as inputs for the non-dimensional form of the model and Equation 22 is used to evaluate the individual's fitness. The chromosomes from the "fittest" individual of the first generation are then used to form a second generation of individuals using methods referred to as reproduction, cross-over, and mutation. During reproduction, the individuals with the best fitness are given the highest probability of having their chromosomes replicated in the coming generation. Though less likely, some of the chromosomes from the least fit individuals can show

up in the next generation to ensure a diverse population. This new population is then crossed and mutated. Cross-over is when two individuals swap single chromosomes and mutations occur where single chromosomes are randomly changed. This keeps the optimization routine from settling around a premature extrema. The second generation is evaluated for fitness and is reproduced, crossed, and mutated into a third generation. The process continues until either the generations stop evolving or some defined limit is reached.

A genetic algorithm using the principles outlined above was adapted from one made available for MatLab by Michael Gordy[19] and uses the methods of Dorsey and Mayer.[20]

Genetic optimization works well to locate the general vicinity of maxima for large parameter set problems. Gradient-based methods can then be used to pinpoint the extrema using the output from the genetic algorithm as a starting point. The ten highest individuals from several trials of the genetic algorithm were used as starting points for MatLab's multi-variable constrained optimization routine `fmincon`. This optimization tool begins at a starting point and calculates the derivative in each direction using either the finite difference method or a user-supplied gradient. The `fmincon` routine searches for a minimum (as opposed to a maximum) so the cost function used in the genetic algorithm had to be inverted. The minima of the inverted cost function is obtained when the change in the derivative falls below a set limit. The locations of extrema from the optimization routine are expressed in non-dimensional groups, implying an infinite combination of circuit elements are possible as long as they satisfy these relations. A single combination of circuit elements from this large pool can be found by substituting in values for z_0, t_0, and one of the following circuit parameters: L_e, L_1, L_2, L_3, or C_1. Since several of the circuit elements are geometry dependent (for example, coil inductance depends on coil geometry), coil and plasmoid dimensions must be fit to them. It must be cautioned that not all parameter combinations from the optimization routines have a physically viable solution. For example, to satisfy the required value for L_3 might require a plasmoid which extends beyond the coils and this is not physically possible in an AFRC. To ensure that a good solution is found, the number of parameter sets selected from the output of the genetic algorithm should be sufficiently large (in this paper, ten sets were chosen) and diverse.

C. Solving the Dimensional Model

A dimensional solution to the optimized scaling relations can be found by substituting in appropriate values for z_0 (coil length), t_0 (plasmoid lifetime), and a circuit element (L_e, L_1, L_2, L_3, or C_1) using the relations shown in Equation 17 - 19. This substitution provides a list of circuit elements C_1, L_e, L_{e1}, L_{e2}, R_e, R_1 and R_2 which can be fixed at their resulting value. The remaining circuit elements are geometry dependent, so the remaining inner and outer coil geometries (radius and cone angle, coil length is equal on both coils and is fixed at z_0) and plasmoid geometry (height, width) must be found so the corresponding inductances and coupling parameters roughly satisfy their expected value. This fitting process is largely done by trial-and-error. A good starting point for this process is to select coil dimensions and estimate their inductance using formularies, such as Lundin,[21] so they come close to L_1 and L_2. These formularies are only valid for low frequency applications less than 1 kHz whereas the discharge frequency for AFRC devices is usually above 10 kHz, but they provide a good estimate.

Once coil dimensions are found so that estimates for L_1 and L_2 are close to their expected value, their frequency-dependent inductance can be calculated with electromagnetic field solvers. These field solvers can also be used to find the plasmoid inductance and the mutual inductance profiles between the coils and plasmoid. The electromagnetic field solvers chosen for this work are from COMSOL's Multiphysics software; a demonstration of how these solvers can be used to find inductance is provided here. In COMSOL, the coil and plasmoid geometry was modeled using a 2D-axisymmetry with a time-harmonic solver, insulative boundary conditions, and an arbitrary cone angle for the outer coil. A "plasmoid" was drawn to occupy a fraction of the space between the inner and outer coils, following the contours of the outer coil. The bounding geometry was made sufficiently large to minimize field disturbances around the coils and plasmoid. The mesh was generated using boundary layer meshing on the inner and outer coils to resolve skin currents and triangular meshing for the rest of the domain. Mesh elements no larger than 0.5 mm along the plasmoid boundary were used. This was the smallest element size that could be used without running out of memory and maintain sufficient resolution. Figure 4 displays a typical geometry with the mesh visible. The conductivity of the plasmoid was set to 30,000 S/m, found with Equation 9 ($\sigma = 1/\rho$) and a plasma temperature of 10 eV. The self-inductance of each inductor L_1, L_2, and L_3 was found by making the other inductors invisible (conductivity of zero) and applying a sinusoidal loop potential ($V_{loop} = 500$ V) to the remaining coil. The frequency for these simulations was calculated from C_1 and the total circuit inductance, using the Lundin

estimated values for L_1 and L_2 ($\omega = 1/\sqrt{(LC)}$). Over a small range of frequencies, inductance does not change significantly so generally this estimated frequency was sufficient. Once the COMSOL simulations were completed, the frequency was recalculated with the new coil inductance values. If it differed from the original frequency by more than 50 percent, the inductance simulations were repeated with the new frequency. After proper boundary conditions, conductivity, frequency, and potentials were applied, the currents and fields were calculated with the electromagnetic solvers. The inductance was then found from inductive impedance: $L = \text{imag}(V_{loop}/I_{tot}\omega)$, where I_{tot} is the integrated current density (total current) in the coil and ω is the frequency of the signal.

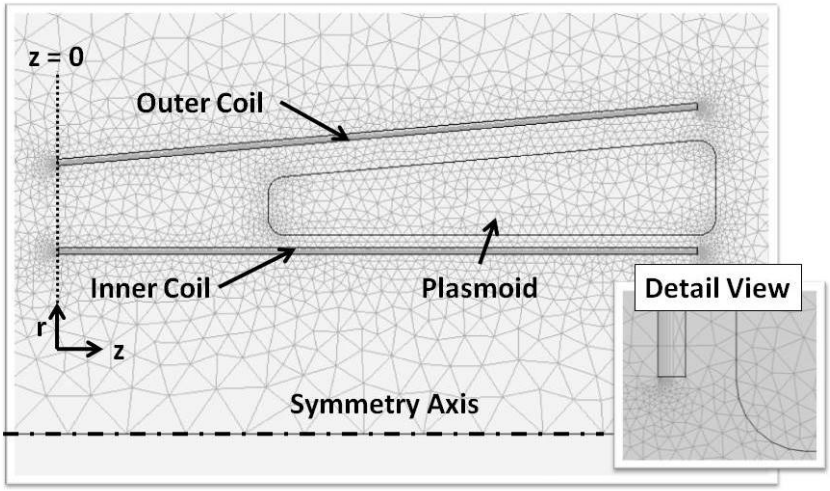

Figure 4. Typical coil mesh and geometry used for COMSOL simulations. The detail view shows the boundary layer mesh used on the coils to resolve skin currents.

The mutual inductance between the coils and plasmoid M_{13}, M_{23} was found by applying a loop potential V_{loop} to only one of the coils. The conductivity of the plasmoid was set to 30,000 S/m and the other coil was neglected (conductivity of zero). The currents and fields were found and the inductance on the coil was calculated from inductive impedance. The current induced in the plasmoid will change the current distribution in the coil, so the inductive impedance in the coil is actually a combination of self inductance of the inner or outer coil L_c (depending on which one was activated), plasmoid L_p, and the mutual inductance M. The three quantities can be related through the following equation:

$$L_{eff} = L_c - \frac{M^2}{L_p} \tag{23}$$

This equation can be verified through a quick circuit analysis and is cited elsewhere.[1,14] To find how the mutual inductance varies with plasmoid position, the plasmoid is moved to a new axial position and the analysis is repeated. A curve fit to the resulting data yields values for the coefficients in Equation 8.

The mutual inductance profile and coil inductances calculated using COMSOL can be supplied to the annular electromagnetic launcher model described by Equations 1 - 7, along with the specified circuit parameters C_1, L_e, L_{e1}, L_{e2}, R_e, R_1 and R_2. Plasmoid mass can be found using the volume of the plasmoid and the plasma density (typically close to 10^{19} particles/m^3). The charging voltage on the capacitor is calculated by inserting C_1, z_0, t_0, and m into the relation for α (Eq. 18). Plasmoid resistance R_3 is found from plasmoid volume and Spitzer resistivity. The model equations with the inputs can numerically integrated to find the currents and plasmoid trajectories. In this work, MatLab's `ode45` numerical integration tool was used. It is an explicit 4th order Runge-Kutta solver, ideal for medium-accuracy, non-stiff problems. Once the plasmoid position and velocity are found, the acceleration efficiency η_{accel} for a plasmoid can be calculated using Equation 10. If the plasmoid's position at $t = t_0$ is less than the coil length z_0, the plasmoid does not translate from the coils so η_{accel} is zero. If η_{accel} is close to ($\pm$ 0.1) or greater than the acceleration efficiency predicted by the optimization routines η^*_{accel}, the coil geometry and circuit elements are considered an acceptable solution. If η_{accel} falls short of η^*_{accel}, a new coil or plasmoid must be selected and the process re-iterated until an acceptable solution is reached.

D. Verification of Numerical Methods and Model

The methods for finding mutual inductance profiles using electromagnetic field solvers was verified by reconstructing the PTX experiment by Martin and Eskridge[14] in COMSOL's Multiphysics software. The PTX experiment used a conical theta pinch coil of 17.5 ° with an aluminum slug to mimic the plasmoid. They measured an effective inductance profile experimentally and calculated one using QuickField software. Repeating their experiment in COMSOL provided the $L_{eff}(z)$ shown in Figure 5. Comparing this profile (labeled in Figure 5 as COMSOL data) to the results obtained by Martin and Eskridge shows good agreement in trend and minimal difference in magnitude. These findings substantiate the computational methods for determining the mutual inductance profile $M(z)$ as outlined previously.

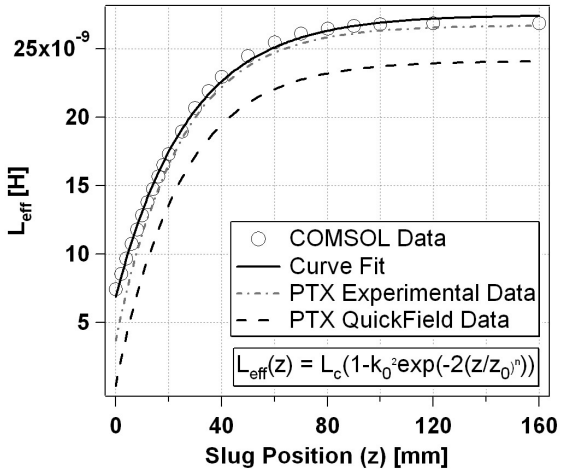

Figure 5. Comparison of effective inductance profiles for the PTX experiment.

Since experimental studies of inductive annular electromagnetic launchers are not available, the annular electromagnetic launcher model was validated in two steps. First, the equations of motion (Equations 1, 2) coupled with the circuit equations (Equations 3, 4, 5, 6, 7) were tested using data published for the ring launcher by Novac.[16] The inner coil circuit was ignored by setting $R_2 = 100\ \Omega$, L_2, $M_{23} = 0$. Setting a high impedance in this branch of this circuit shunts 99.99 percent of the current through the outer coil circuit and the circuit behaves as if the inner coil were not there. The remaining parameters were set to values from Table 1 in Novac:[16] $m = 0.7$ g, $C_1 = 31.8\ \mu F$, $L_e = 12.7$ nH, $R_e = 1$ mΩ, $L_1 = 63.6$ nH, and $L_3 = 74.7$ nH. The projectile resistance R_3 was set to 15 mΩ and the capacitor charged to 30 kV. The mutual inductance profile was not specified, but Martin and Eskridge who performed a similar validation study for a model they developed used $k_0 = 0.98$, $z_0 = 5$ mm, $n = 1$, and $z_s = 0$ with good results. The annular electromagnetic launcher model with these parameters determined the final projectile velocity to be 3.78 km/s, near the 4 km/s terminal velocity reported by Novac. This validation step was done for both the non-dimensional and dimensional form of the model.

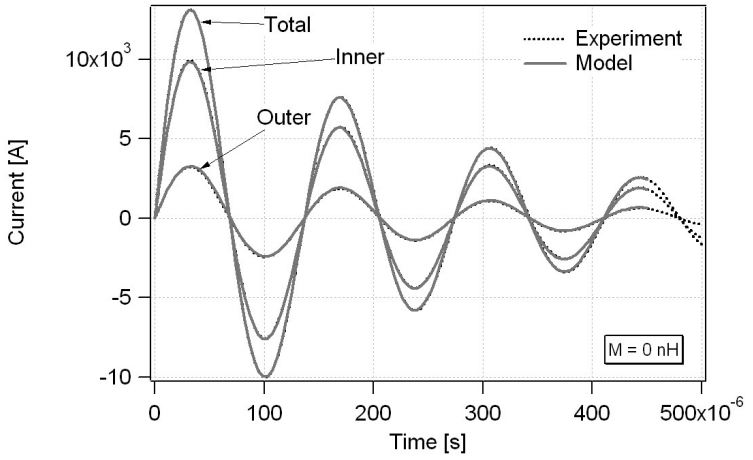

Figure 6. Comparison of circuit currents I_0, I_1, I_2 with XOCOT-T experimental data.

Following validation of the equations of motion, the coil circuit equations (Equations 3, 4, 5, 7) were tested using circuit parameters from the XOCOT-T.[4] These include: $V_c = 1444$ V, $C = 225\ \mu$F, $L_e = 1.53\ \mu$H, $R_e = 16$ mΩ, $L_1 + L_{e1} = 2.29\ \mu$H, $L_2 + L_{e2} = 746\ \mu$H, $R_1, R_2 = 1$ mΩ. The coil, transmission line, and external inductances for the XOCOT-T were measured with an Agilent 4294A Impedance Analyzer. The external resistance R_{ext} was adjusted to match the damping on the experimental data, since this value was

not measured. The circuit equations (Equations 3, 4, 5, 7) were solved to find I_0, I_1, and I_2. These were compared to measurements from Pearson current monitors on the XOCOT-T experiment. As is shown in Figure 6, exceptional agreement between the experimental data and the circuit solutions was found. This, combined with the launcher model validation outlined in the previous paragraph, shows that the annular electromagnetic launcher model should provide fairly reliable results.

V. Preliminary Results and Discussion

The optimization methodology detailed above was demonstrated by running a test case. Though the results are preliminary, they indicate that the methodology presented in this paper can result in a physically-realizable geometry. The test case was started by using the genetic algorithm routine written in MatLab to find parameter combinations with $\eta^*_{accel} \geq 0.5$ for the non-dimensional form of the annular electromagnetic launcher model. Upper bounds and lower bounds for the non-dimensional parameter space were defined as shown in Table 1. An initial guess was also provided. This was used as the chromosome set for one individual of the first generation. The remaining individuals were randomly seeded.

Table 1. Parameter Space Definitions for the Genetic Algorithm

parameter	θ_1	θ_2/θ_1	θ_3/θ_1	γ_e	γ_p	α	τ_0	k_{13}	k_{23}	σ_{13}	σ_{23}/σ_{13}
upper	10	0.5	0.5	1	1	1000	5	0.7	0.7	2.0	1.1
lower	0.001	0.001	0.001	10^{-4}	10^{-4}	0.001	0.001	0.1	0.1	0.1	0.9
initial	1.0	0.01	0.01	10^{-4}	10^{-4}	0.001	0.01	0.55	0.55	0.2	1.0

	n_{13}	n_{23}	θ_{e1}	θ_{e2}	γ_1	γ_2	σ_{s13}	σ_{s23}
upper	3.0	3.0	1.0	1.0	1.0	1.0	0.01	0.01
lower	1.0	1.0	0.001	0.001	10^{-4}	10^{-4}	10^{-4}	10^{-4}
initial	1.0	2.5	0.001	0.001	10^{-4}	10^{-4}	10^{-4}	10^{-4}

Table 1 shows the default settings; three different trials were performed with the upper bound of α set to 100, 500, and 5000. Each trial was started using a population size of 20 individuals per generation. Dorsey and Mayer suggest a population size of 24, however anything greater than 20 increased the total computation time extensively. The individual with the highest efficiency from each generation was stored until an individual with a higher fitness was found. To decrease the time to convergence, every 50 iterations a random individual was replaced by this fittest individual. The simulation was stopped when the efficiency did not increase by 10^{-4} in 2000 consecutive generations. The algorithm created over 16,000 generations, taking 116 hours to complete. A depiction of how the generations evolved over the course of the simulation can be shown in Figure 7, where the best efficiency from every 10th generation is plotted. By following the highest markers for each generation, it can be noticed how total efficiency increases over time before the solution terminates at $\eta^*_{accel} = 0.69$. While the overall fitness of the entire population increases with generation, there are still many generations with η^*_{accel} significantly below the leading η^*_{accel} as evidenced by the abundance of markers in the $\eta^*_{accel} = 0.2$ to $\eta^*_{accel} = 0.5$ region. From this, it appears that the generations do not evolve as quickly as they could. Speculation for why this happens is still preliminary, but it is thought that this could be caused by a high mutation rate or it could be due to the highly irregular nature of the fitness function. Further investigations into why this occurs as well as methods for reducing the computation time are necessary.

Each individual with an efficiency of greater than 0.5 was saved during the genetic algorithm routine. When the routine completed, these individuals were sorted according to efficiency and the ten fittest individuals from each trial were passed to the `fmincon` solver for the second round of optimization. For the trial shown in Table 1, all the top 10 individuals had an efficiency close to 0.69. They emerged from the second optimization round with efficiencies of 0.75, deviating from this by less than 0.0001. The small deviation indicates they are all fair solutions with regard to maximum efficiency; it is difficult to single out one solution based on efficiency. Not all the individuals generated during the second optimization round were physically viable solutions; though reasonable bounds were placed on the non-dimensional terms shown in Table 1, some of the results from the optimization routines were geometry combinations that are not

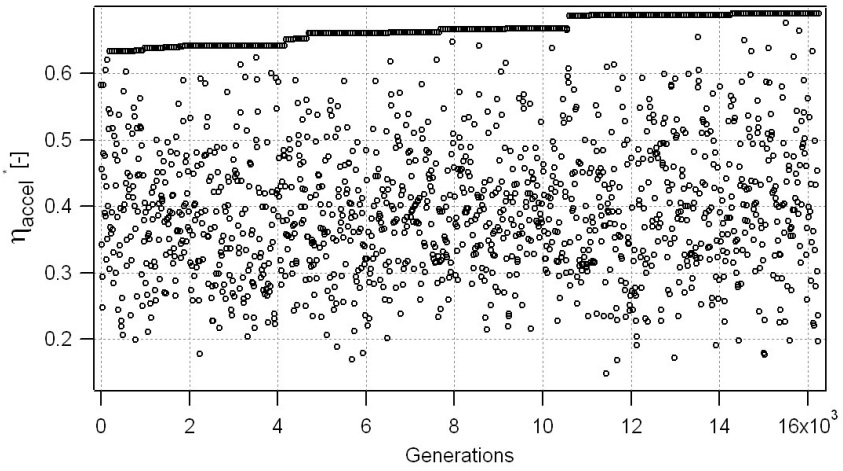

Figure 7. Evolution of the genetic algorithm over 16,000 generations. The efficiency of each generation is plotted. Every 10th generation is shown for clarity.

physically possible. These were discarded and one individual out of the remaining individuals was chosen for further investigation. The non-dimensional parameter set from this individual is displayed in Table 2, as the "target" individual. For this individual, $\eta^*_{accel} = 0.753$.

The target individual's parameter set was put into dimensional terms by choosing the coil length and plasmoid lifetime: $z_0 = 12$ inches and $t_0 = 20$ μs. The outer coil inductance L_1 was also fixed by choosing the coil to have a 5 inch radius and a single turn. From Lundin's formulary,[21] the inductance of this coil is approximately 152 nH. Using Equations 17 - 19 with the values shown in row 1 of Table 2, the following circuit elements were calculated: C_1 = 1,400 μF , L_e = 15.2 nH, R_e, R_1, R_2 = 0.33 $\mu\Omega$, and L_{e1}, L_{e2} = 15.2 pH. These inductances and resistances are lower than can probably be achieved in a physical circuit, since external inductances are usually 40 - 100 nH and resistances are typically slightly under 1 mΩ. As can be noticed from Table 2, peak efficiency happens when the scaling relations for these parameters hit their lower bound. Future studies should adjust the lower bounds on these parameters to a more appropriate level. Continuing with these parameters for demonstration purposes, a coil and plasmoid geometry must be found to sastify the remaining target values. Unfortunately, this must be accomplished using trial-and-error. As a starting point, it was decided that the coil dimensions would be fixed and several different cone angles from 1 $^\circ$ up to 15 $^\circ$ would tested. With the dimensions of the outer coil set to a radius of 5 inches and length of 12 inches, the inner coil should have a radius of 3.35 inches so that $L_2 = 0.5L_1$ (see Table 2). The outer and inner coil were modeled in COMSOL and plasmoid was drawn between them to be 70 percent of the annulus width and annulus height. The coil inductances, plasmoid inductance, and mutual inductance profiles $M_{13}(z)$ and $M_{23}(z)$ were found from inductive impedance. Curve fits to the data for $M_{13}(z)$ and $M_{23}(z)$ yield the coefficients described in the equations. Since plasmoid resistance and plasmoid mass depend on plasmoid volume, these values were recalculated in-situ for each cone angle. Also, since $\alpha = (C_1V_c^2)/(mu_0^2)$, V_c also needed to be recalculated for each cone angle. As a sample, at a cone angle of 5 $^\circ$, m = 2.25 x 10^{-8} kg (plasma density of 3 x 10^{19} m^{-3}), R_3 = 0.14 mΩ (conductivity of 30,000 S/m), and V_c = 1.0 kV. The new values for L_1, L_2, and L_3, along with M_{13} and M_{23} were inserted into Equations 1 - 7. MatLab's `ode45` solver then calculated the coil currents and plasmoid trajectories at each cone angle. Acceleration efficiency was found for each plasmoid that was able to leave the coils during t_0. The results are plotted in Figure 8.

Acceleration efficiency depends strongly on the cone angle, as in apparent in Figure 8. This can be understood by examining Equation 1. Maximizing the kinetic energy of the plasmoid requires that the plasmoid reaches the axial location of peak dM/dz at the same time the coil currents peak. The peak dM/dz occurs right outside the ends of the coils, where the magnetic field diverges the greatest. Too small of a cone angle will keep the plasmoid from reaching this region during peak coil current and too large of a cone angle will eject the plasmoid before the peak currents develop. The cone angle that best matches the target efficiency is at 5 $^\circ$ apparent from Figure 8. This solution has $\eta_{accel} = 0.79$.

Since the objective of this demonstration was to find scaling relations which result in the highest efficiency

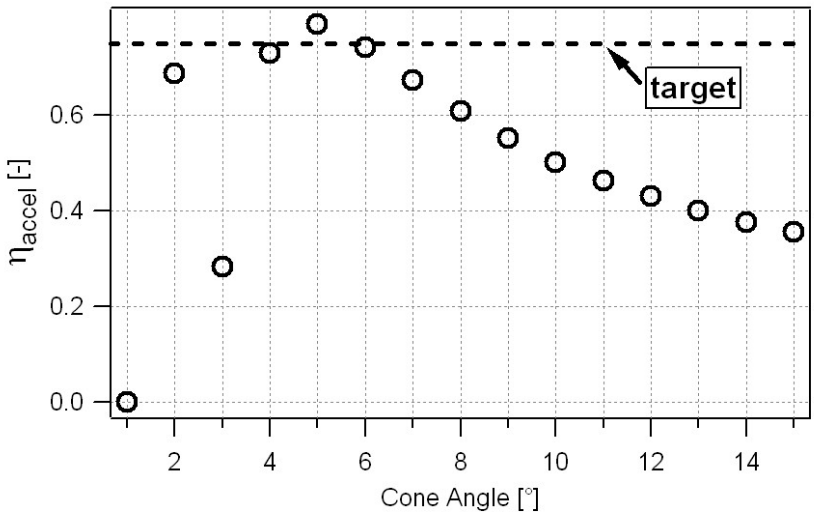

Figure 8. Acceleration efficiency for different cone angles for dimensional study. The dashed line represents the target efficiency from the optimization routines.

Table 2. Comparison of Parameter Set from Optimization Studies and Dimensional Studies

parameter	θ_1	θ_2/θ_1	θ_3/θ_1	γ_e	γ_p	α	τ_0	k_{13}	k_{23}	σ_{13}	σ_{23}/σ_{13}
target	10	0.5	0.4944	10^{-4}	10^{-4}	273.04	4.3264	0.7	0.7	1.4429	1.0470
case 5	11.0	0.43	0.77	10^{-4}	0.04	273.04	4.3264	0.76	0.72	1.05	1.10
change	0.1	-0.15	0.56	0	407	0	0	0.08	0.03	-0.27	0.05

	n_{13}	n_{23}	θ_{e1}	θ_{e2}	γ_1	γ_2	σ_{s13}	σ_{s23}
target	2.06	2.80	0.001	0.001	10^{-4}	10^{-4}	7.64 x 10^{-4}	0.0046
case 5	2.21	3.04	0.001	0.001	10^{-4}	10^{-4}	0	0.13
change	0.07	0.09	0	0	0	0	-1	27.66

and see if a physical solution can be found to satisfy these relations through trial and error, it is useful to compare the target parameters with the physical solution. The circuit parameters used to obtain the results shown in Figure 8 at 5 ° (Case 5), were converted back into non-dimensional terms using the scaling relations shown in Equations 17 - 19. The comparison is shown in Table 2. Most of the candidate parameters differ from the target parameters by less than 30 percent. Though plasmoid resistance γ_P and plasmoid inductance θ_3 from the dimensional simulation is significantly higher than the optimal found by the optimization study, it is not enough to decrease the acceleration efficiency. The relative plasma inductance θ_3 and coupling coefficients k_{13} and k_{23} for the dimensional simulation (candidate solution) exceed the limits placed on the optimization routine, as is shown in Table 2. For the optimization study, these limits were set as "soft" limits or regarded as limits that technology and experimental design probably could not exceed. With the dimensional study, it is shown that it is possible to slightly exceed these limits and when it happens, it results in a greater than expected efficiency.

The optimization routine found that the maximum efficiency happens when θ_1, θ_2, θ_3, k_{13} and k_{23} approach the upper limit and γ_E, γ_p, γ_1, γ_2, θ_{e1}, and θ_{e2} are minimal. This result should come as no surprise. The first group of terms maximizes the amount of energy from the capacitor which can be transferred to the coils and the last group of terms remove energy from the circuit without providing any acceleration to the plasmoid. With confirmation of how these terms affect efficiency, it would be instructive to fix these terms at their appropriate limits and conduct further optimization studies on the remaining terms to see how they impact solution.

As previously stated, the purpose of this preliminary exercise was to demonstrate the application of an

optimization routine to the annular electromagnetic launcher model. Though this exercise requires further refinement and investigation, the preliminary findings indicate that it is possible to obtain meaningful results from these methods and close to the target efficiency. Most of the values obtained from the dimensional study come within 30 percent of the target value. This is exciting when one considers following discussion. The AFRC setup is a dynamic system where the circuit elements and coil geometries strongly influence each other's behavior. For instance, the outer coil is an inductor and therefore contributes to the discharge frequency, which through the skin effect dictates how the currents are distributed in the coils. The current distribution will change the inductance of the coil, the inductance of the total system, and the coupling of the coils and plasmoid (k_{13}, k_{23}, z_{13}, z_{23}, z_{s13}, z_{s23}). Therefore, it is impossible to change one element of the setup without other elements changing. The optimization routine does not consider this dynamic behavior and independently selects parameters that will result in the best efficiency for the system. Once a final verdict is reached, a circuit and geometry must be fit to the outcome of the optimization routine. It is entirely likely that the parameters selected by the optimization will not have a physical solution (for example, the plasmoid might have to extend beyond the coils to achieve the target inductance). Having evidence that a viable solution can be reached promotes further development of this approach.

VI. Conclusion

An annular electromagnetic launcher model has been developed to predict the translation physics of an AFRC plasmoid. This model has been optimized for peak efficiency using a combination of methods. Non-dimensionalization of the model provides scaling relations between model parameters to obtain a generalized solution. The non-dimensional form of the model was put into a genetic algorithm to find the relative location of local maxima. These parameter sets were then re-optimized using a gradient based solver (`fmincon` in MatLab) to pinpoint the maximum efficiency. A set of dimensional parameters was fit to one of the scaling relation sets from the optimization round. The annular electromagnetic launcher model was then used to find the efficiency of this dimensional parameter set. The result of $\eta_{accel} = 0.79$ closely matched the predicted value from the optimization round $\eta^*_{accel} = 0.75$. The preliminary results of these studies indicate that it is possible to find a coil and plasmoid geometry to obtain the peak efficiency predicted by the optimization techniques. However, further refinement of the results are necessary before accurate efficiency predictions can be made.

VII. Future Work

The annular electromagnetic launcher model combined with the optimization routines presented in this paper is in the preliminary stage of investigation. Further work on this optimization can find ways to reduce the computation time and increase the number of useful data sets from the optimization process. Sensitivity studies on the results can be done to show how certain parameters contribute to the overall efficiency. This model is based on information about the AFRC plasmoid that is not readily available. Experiments on stationary plasmoids are necessary to get more information about plasma temperatures, densities, and plasmoid shapes. Finally, experimental studies on AFRCs are necessary to validate the model and provide information about AFRC plasmoid translation which is not treated in this model (plasmoid expansion, magnetic fields, etc).

VIII. Acknowledgments

The authors would like to thank Dr. Gordon Parker (Mechanical Engineering-MTU) for sharing his expertise in numerical optimization and Dr. Warren Perger (Electrical Engineering-MTU) for providing the computational resources. The authors also wish to acknowledge and thank Dr. Brian Beal (AFRL-Edwards AFB) for his contributions, support, and technical suggestions. This work was conducted under DOD contract FA9300-06-C-0023.

References

[1]Dailey, C. L. and Lovberg, R., "The PIT MkV Pulsed Inductive Thruster," NASA Contractor Report 191155, July 1993.
[2]Koelfgen, S., Hawk, C., Eskridge, R., Lee, M., Martin, A., and Smith, J., "A Plasmoid Thruster for Space Propulsion,"

Proceedings of the 39th Joint Propulsion Conference and Exhibit, No. AIAA-2003-4992, Huntsville, AL, July 2003.

[3]Kirtley, D. E., *Study of the Synchronous Operation of an Annular Field Reversed Configuration Device*, Phd thesis, University of Michigan, Ann Arbor, MI, 2008.

[4]Niemela, C. S. and Kirtley, D. E., "Initial Results on an Annular Field Reversed Configuration Plasma Translation Experiment," *Proceedings of the 6th MS/4th LPS/3rd SPS Joint Subcommittee Meeting*, No. TP-2008-489, JANNAF, Orlando, FL, December 2008, Distribution A.

[5]Phillips, J., "Proposal to Produce Large Compact Toroids," Report LA-8711-P, Los Alamos National Laboratory, March 1981.

[6]Pierce, W., Maqueda, R., Brooks, R., and Farengo, R., "Initial Results from Parallel Coil Operation of the Coaxial Slow Source Field Reversed Configuration Device," *Nuclear Fusion*, Vol. 33, 1993, pp. 117–132.

[7]Pietrzyk, Z., Vlases, G., Brooks, R., Hahn, K., and Raman, R., "Initial Results from the Coaxial Slow Source FRC Device," *Nuclear Fusion*, Vol. 27, No. 9, 1987, pp. 1478–89.

[8]Berger, R., *Analysis of Slow Formation of Plasmas in a Coaxial Double Theta Pinch*, Phd thesis, University of Washington, 1993.

[9]Smith, R. J., *Magnetic Equilibria of the Coaxial Slow Source*, Ph.D. thesis, University of Washington, 1989.

[10]Tuszewski, M., "Field Reversed Configurations," *Nuclear Fusion*, Vol. 28, 1988, pp. 2033–2092.

[11]Rej, D. J., Armstrong, W. T., Chrien, R. E., Klingner, P. L., Linford, R. K., McKenna, K. F., Sherwood, E. G., Simeon, R. E., Tuszewski, M., and Milroy, R. D., "Experimental studies of field-reversed configuration translation," *Physics of Fluids*, Vol. 29, No. 3, Mar 1986, pp. 852–862.

[12]Intrator, T. P., Wurden, G. A., Sieck, P. E., Waganaar, W. J., Renneke, R., Dorf, L., Kostora, M., Hsu, S. C., Lynn, A. G., Gilmore, M., Siemon, R. E., Awe, T., Degnan, J., Grabowski, C., and Ruden, E. L., "Physics basis and progress for a translating FRC for MTF," *Journal of Fusion Energy*, Vol. 27, No. 1-2, 2008, pp. 57–60.

[13]Jahn, R. G., *Physics of Electric Propulsion*, Dover Publications, Mineola, NY, 1968.

[14]Martin, A. and Eskridge, R., "Electrical coupling efficiency of inductive plasma accelerators," *Journal of Physics D-Applied Physics*, Vol. 38, No. 23, 2005, pp. 4168–4179.

[15]Polzin, K. A. and Choueiri, E. Y., "Performance optimization criteria for pulsed inductive plasma acceleration," *IEEE Transactions on Plasma Science*, Vol. 34, No. 3, 2006, pp. 945–953.

[16]Novac, B. M., Smith, I. R., Enache, M. C., and Senior, P., "Studies of a very high efficiency electromagnetic launcher," *Journal of Physics D-Applied Physics*, Vol. 35, No. 12, 2002, pp. PII S0022–3727(02)33567–8.

[17]Cassibry, J. T., "Comparison of Directly and Inductively Coupled Pulsed Electromagnetic Thrusters," *IEEE Transactions on Plasma Science*, Vol. 36, No. 5, 2008, pp. 2180–2188.

[18]Spitzer, L. J., *Physics of Fully Ionized Gases*, Vol. 3 of *Interscience Tracts on Physics and Astronomy*, Interscience Publishers, Inc., New York, 1956.

[19]Gordy, M., http://www.geatbx.com/links/genetic maximization matlab m gordy.html.

[20]Dorsey, R. E. and Mayer, W. J., "Genetic Algorithms for Estimation Problems with Multiple Optima, Nondifferentiability, and other Irregular Features," Amer Statist Assn, 1995, pp. 53–66.

[21]Lundin, R., "A handbook formula for the inductance of a single-layer circular coil," *Proceedings of the IEEE*, Vol. 73, No. 9, 1985, pp. 1428–1429.